Research article

Yulong Fan, Yunkun Xu, Meng Qiu, Wei Jin, Lei Zhang, Edmund Y. Lam, Din Ping Tsai and Dangyuan Lei*

Phase-controlled metasurface design via optimized genetic algorithm

https://doi.org/10.1515/nanoph-2020-0132
Received February 18, 2020; accepted April 14, 2020; published online June 25, 2020

Abstract: In an optical Pancharatnam-Berry (PB) phase metasurface, each sub-wavelength dielectric structure of varied spatial orientation can be treated as a point source with the same amplitude yet varied relative phase. In this work, we introduce an optimized genetic algorithm (GA) method for the synthesis of one-dimensional (1D) PB phase-controlled dielectric metasurfaces by seeking for optimized phase profile solutions, which differs from previously reported amplitude-controlled GA method only applicable to generate transverse optical modes with plasmonic metasurfaces. The GA–optimized phase profiles can be readily used to construct dielectric metasurfaces with improved functionalities. The loop of phase-controlled GA consists of initialization, random mutation, screened evolution, and duplication. Here random mutation is realized by changing the phase of each unit cell, and this process should be efficient to obtain enough mutations to drive the whole GA process under supervision of appropriate mutation boundary. A well-chosen fitness function ensures the right direction of screened evolution, and the duplication process guarantees an equilibrated number of generated light patterns. Importantly, we optimize the GA loop by introducing a multi-step hierarchical mutation process to break local optimum limits. We demonstrate the validity of our optimized GA method by generating longitudinal optical modes (i. e., non-diffractive light sheets) with 1D PB phase dielectric metasurfaces having non-analytical counter-intuitive phase profiles. The produced large-area, long-distance light sheets could be used for realizing high-speed, low-noise light-sheet microscopy. Additionally, a simplified 3D light pattern generated by a 2D PB phase metasurface further reveals the potential of our optimized GA method for manipulating truly 3D light fields.

Keywords: dielectric metasurface; genetic algorithm; light sheet; optical Pancharatnam-Berry phase.

1 Introduction

Optical metasurface, an optically thin layer consisting of sub-wavelength plasmonic or dielectric structures, is capable of tailoring the wave front of the outgoing light waves by introducing an abrupt phase discontinuity in the transverse plane, thus deflects the incident light in a customized angle owing to the generalized Snell's law [1]. The special output light beams can be freely harnessed by the phase discontinuity serving as a degree of freedom that can be engineered by the artificial periodic structures of optical metasurface. In the last decade, the continuous development of nanofabrication technologies was the main driving impetus that has advanced and enriched the bourgeoning research field of optical metasurfaces, triggering plethora of applications such as optical metalens [2–9], beam splitter [10–12], integrator [13–15], differentiator [13, 15–17], Stokes parameters extractors [18–20], hologram [10, 21–28], special light beam generators [10, 29–38], and etc. Among all the diverse metasurfaces, the optical PB phase metasurfaces have attracted more and more interests of scientists owing to their high degrees of freedom by easily rotating the orientation of the unit cells, and their high conversion efficiency due to the low dielectric loss [2, 3, 10, 23, 27, 38, 39]. Another advantage of optical PB phase metasurface is the identical optical

*Corresponding author: Dangyuan Lei, City University of Hong Kong, Department of Materials Science and Engineering, Kowloon, Hong Kong, China, E-mail: dangylei@cityu.edu.hk
Yulong Fan and Yunkun Xu: City University of Hong Kong, Department of Materials Science and Engineering, Kowloon, Hong Kong, China. https://orcid.org/0000-0002-6841-9348 (Y. Xu)
Meng Qiu and Wei Jin: The Hong Kong Polytechnic University, Department of Electrical Engineering, Hung Hom, Hong Kong, China
Lei Zhang: The Hong Kong Polytechnic University, Department of Computing, Hung Hom, Hong Kong, China
Edmund Y. Lam: The University of Hong Kong, Department of Electrical and Electronic Engineering, Pokfulam, Hong Kong, China
Din Ping Tsai: The Hong Kong Polytechnic University, Department of Electronic and Information Engineering, Hung Hom, Hong Kong, China

transmission of each unit cell, which can be treated as an array of point sources with identical amplitude but different phases. Whereas, all the aforementioned conventional optical metasurfaces are designed on the basis of analytical solutions of specific optical modes, or by hologram method, so that the potential of the optical metasurfaces may be underestimated and might be further explored, e. g., by machine learning method.

The surge of artificial intelligence (AI) begins changing everyone's daily life by its powerful data processing and potential deep learning ability, and thus potentially shows a new paradigm in the area of scientific research. Since several years ago, scientists have begun to exploit the possibilities of using genetic algorithm (GA, also named evolutionary algorithm) to code metasurfaces in order to find unprecedented non-analytical and non-intuitive solutions for optical metasurface synthesis [40–49]. Very recently, AI based on neural network algorithms mimicking the functionalities of the neurons of a biological brain to understand, connect, and predict solution to a problem from a large set of examples, have also been applied to study the electromagnetic resonance properties of complex metallic structures before subsequent synthesis of the optical metasurfaces [50–56].

Distinct from the amplitude-controlled GA investigated in Ref. [40–49] or the complex meta-dielectric resonance structures studied in Ref. [50–56], here, we address a new phase-controlled GA method targeting on-demand optical PB phase metasurface synthesis. The special characteristic of high degree of freedom of PB phase metasurfaces requires a high-quality mapping function between point sources at the rear of the metasurface and the optical field formed afterward using integral of Green function, and a special fitness function to efficiently evaluate each design and then sort them according to scores. Furthermore, an appropriate mutation process is of great importance to efficiently drive the GA process towards right direction of evolution, and allows the candidates to escape from the local optima, which is a problem that often occurs in GA programming. Besides, special attention should be paid to the additional phase induced between every adjacent unit cell since large additional phase θ, will degrade the transmission efficiency when $\theta < k^*d$ (k is wave vector and d is spacing between adjacent unit cells) [33], or lead to the occurrence of total reflection when $\theta > k^*d$ according to generalized Snell's law [1, 41, 43], though arbitrary phase attributed to each unit cell can be freely chosen in theory in the Green function mapping process. The GA-obtained phase profile can be later used to construct a 1D PB phase metasurface by rotating the orientation of dielectric unit cells.

The light sheet mode employed in this paper to verify the validity of our optimized GA, is broadly utilized in cell biology, anatomical sciences, and neurosciences [57–59]. It's worthy to be noted that unlike conventional metasurfaces mainly relying on the analytical solutions of special optical modes or on hologram solutions in the transverse plane of propagating waves, a light sheet mode generator will give rise to a quasi-uniform intensity distribution in the long range of propagating direction and thus eliminates the possibility of seeking for the analytical solutions due to the continuous varying of optical phase (except for Bessel beam launcher [32, 33]). Of course, the light sheets created by our optimized GA design including but not limited to Bessel like optical modes, can hardly find analytical solutions, if not impossible.

2 Methods

2.1 Mathematical methods

An appropriately efficient mapping function needs to be created aimed to efficiently calculate the optical field at each sampling point during the mutation process. The PB phase unit cells are subwavelength elements thus can be treated as point sources with identical amplitude but variable optical phases. To this end, Matlab programming based on the Huygens–Fresnel principle [60] using Green function is exploited in this study, and a server with Intel(R) Xeon(R) CPU E5-2620 v3 @ 2.30GHz (36 cores, 72 threads) and 256 GB memory was employed. During the GA calculation for the 1D metasurface design, we observed the consumption of 30 GHz for CPU and 1 GB memory.

2.2 Metasurface and sampling

Our target optical function is light sheet mode and the elements in PB phase metasurface are presumed to vary only in x direction while keeping the same in y direction, thus the profile in xz plane of the optical field are chosen to judge the quality of the metasurface (see in Figure 1A). Equi-spacing sampling points in both "Dark Region" and "Bright Region" are utilized to efficiently evaluate the quality of the DNAs of the population. Obviously, a DNA showing less intense light in the "Dark Region" and more intense light in the "Bright Region" is regarded as a better light sheet pattern and will be selected to duplicate and mutate for the next generation. 16×34 monitors are set in the study of 2D metasurface design.

2.3 GA process

As every unit element is individually tunable, optical PB phase metasurface with N elements has N degrees of freedom. This results in an exponential growth of number of possible states as the increase of the number of elements, and lead to extremely long time spent by classical algorithms, such as enumeration, to solve this kind of problem.

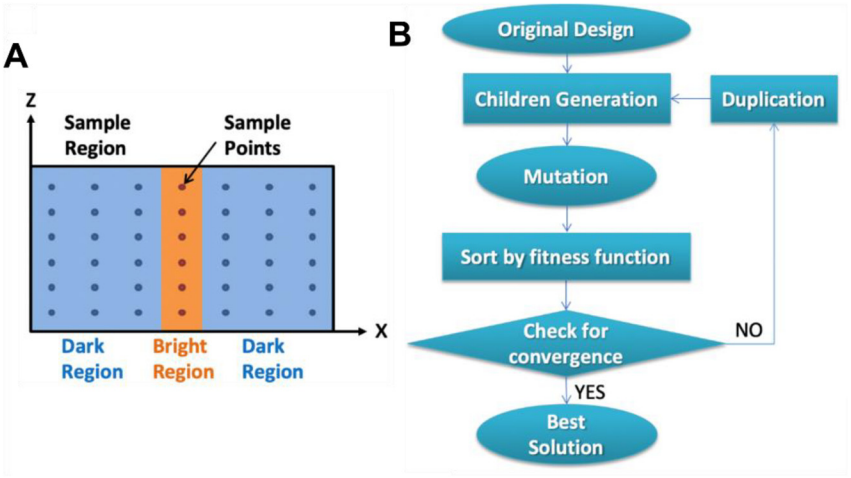

Figure 1: The targeted light sheet mode and sampling with an array of equi-spaced points inside (Bright Region) and outside (Dark Region) the light-sheet pattern (A); Flow chart of GA includes initialization of an original generation, application of mutation to the current generation, sorting the children generation according to their scores graded by fitness function, and duplication of the screened children if the score diverges, until the cyclic loop ends up when the ending condition is fulfilled (B).

Genetic algorithm (GA), stemming from Darwin's theory of evolution, however, is intentionally designed to seek for high-quality solutions to optimization and searching problems. This method is especially less time consuming and suited for problems dealing with large numbers of degrees of freedom with non-analytical solutions. Our genetic algorithm consists of several main cyclic steps as shown in Figure 1A. Akin to natural selection process, GA will firstly initialize a population as the original generation. Then the loop is triggered with the mutation of the current generation and subsequently, a fitness function will evaluate every individual and the population is screened for good features (high score). The screened individuals are selected as parents to generate the next generation (duplication in Figure 1A) while the others are eliminated. GA will keep cycling this process until the screened population fulfils the ending conditions when the scores converge. It's worthy to be noted that a "Duplication" process is indispensable to ensure the balance of the population (the same number as the initial generation). Although mutation occurs at every moment in nature, it's usually only introduced in one single phase in the GA process for convenience.

2.3.1 Initialization: A widely used well-chosen initial condition instead of a random pattern will largely shorten the time consumed by GA process. A plane wave focused by hyperbolic lens [61, 62] as well as other sorts of lenses such as the most studied spherical lens or axicon can be chosen as the initial pattern of the metasurface. In this work, the hyperbolic lens profile is assigned to every DNA as their initial characters and is expected to grow longer and longer under the supervision of the selection rule during GA process.

2.3.2 Mutation: Mutation process exerts a heavy influence on the GA calculation efficiency, and meanwhile determines the stability of the population during GA process to some extent. It's worthy to be noted that the crossover process doesn't exist in this study, in consequence of the absence of an expected predefined target design (longer the better, with reasonable full-width-half-maximum, FWHM). The disadvantage of crossover without target design in our case is that the huge numbers of freaks and very low percentage of good individuals in the children generation will give back the massive data that needs to be evaluated by fitness function and will largely slow down the mutation process. Consequently, in order to efficiently propel the GA process towards good direction of evolution thus largely shorten the time consumption, a high mutation rate should be chosen for the Matlab programming. Contradictorily, a too large mutation rate will also harm the GA, because it gives a big probability for the children to escape from a local optimum to go back to a worse point due to the lack of crossover process, then the number of high-quality individuals will be less and less. In the most possible situation, this will lead to an unstable population number and an endless GA loop. To balance the processing efficiency and meanwhile avoid the unstable population, a reasonably big mutation rate 0.3 is chosen in this study. Another important factor should be taken into consideration is the mutation extent. The weakness of a small mutation extent is that the children are highly likely to be trapped in one of the local optimum points near the start point and they can never reach the best solution. While the disadvantage of a large mutation extent will allow the children to quickly escape from the local optimum points near the start point, and the children will probably disperse in several different local optimum points far from the start point, because they cannot reach the best solution point with the large mutation extent as the fitness function cannot make the decision which child is the best one. We overcome this problem by introducing a multi-step GA process with different mutation extent to allow the children to escape from the optimum points close to the start point but also reach the best solution (see in section 2.3.4. Approach towards global optimal solution).

2.3.3 Fitness function: A fitness function is elaborately chosen to be responsible for evaluating the quality of a light-sheet mode, whose quality is of great importance to determine the selection direction and the final DNA of the GA process, especially in the absence of predefined target design and the crossover process. Akin to the natural selection or artificial selection process, slightly different selection directions may result in large different biological characters, just like Darwin's finches and Galapagos penguin. Here the chosen fitness function is composed of several characters to judge the quality of light field, as shown in the following equation:

$$\begin{aligned}\text{Score} = &-\text{Sum}(\text{Deviation with best})*a_1 + \text{Mean}(\text{Light region})*a_2 \\ &-\text{Std}(\text{Light region})*a_3 + \text{Min}(\text{Light region})*a_4 \\ &\text{Max}(\text{Light region})*a_5 - \text{Max}(\text{Dark region})*a_6\end{aligned}$$

where a_1 to a_6 are empirical coefficients with different weighs on the Score function; "Sum(Deviation with best)" stands for the intensity

deviation between the current light field and the best one among all the already solved ones; “Mean(Light region)”, “Std(Light region)”, “Min(Light region)” and “Max(Light region)” represent the mean, standard deviation, minimum and maximum values of the intensity in the bright region, and the Max(Dark region), the maximum value of intensity in dark region. In this work, only the equi-spaced feature points are chosen to be calculated using Green function and graded using Score function, in order to accelerate the GA process.

2.3.4 Approach towards global optimal solution: A multi-step hierarchical GA process with different mutation extents is employed to help children escape from the local optimum near the start point and approach to the global optimal solution: the first GA process with large mutation extent is set to screen for the children in the local optima far from the start point. The corresponding DNAs of the children are returned as the initial condition for the second GA process with small mutation extent to screen for the global optimal solution. After the convergence of the first GA process, there is strong possibility that the population will give back several design results located inside the local optimum points where the fitness function is not able to determine which one is the global optimal. While, all the children will be found in one single optimum point, namely the global optimal point, when smaller and smaller mutation extents are assigned to the GA process during this multi-step mutation process. Normally there should be only one global optimal solution in each specific design when the mutation direction is selected and determined by the fitness function.

2.3.5 Mutation boundary: Demanded by generalized Snell’s law, the additional phase should not exceed k*d, or the metasurface will give a rapid rise to the total reflection and may result in a strong scattering. The prominent difference between the calculation and simulation results comes from the fact that in Matlab calculation, every PB phase unit cell is presumed to be an isolated point source with arbitrary phase and its neighbors would not exert an impact on its independence, so the DNA can have any phase profile a priori. But some of them are indeed not allowed in FDTD simulations when the phase difference of adjacent unit cells is large enough to give rise to a giant total reflection or scattering, which result in a low (even no) light transmission across the metasurface. Then, the equivalence between the point sources and the metasurface breaks down and leads to the giant difference between the two results. To avoid this side effect, a mutation boundary is created to exert the phase change limit of adjacent unit cells of conventional metasurfaces ($\pi/2$ as usual) on the DNA mutation process. During the GA process, when a unit cell of one DNA is chosen to mutate, a random phase change value amongst the mutation extent is added to the current phase. The new phase should be subsequently compared with the phases of its neighbors under supervision of a judge sentence. If any of the difference exceeds $\pi/2$ (other threshold is also possible), the phase of this unit cell will be pulled back to the maximum value that is acceptable by the threshold.

3 Result and discussion

We begin this part with discussing the influence of mutation boundary. An example is illustrated in Figure 2, where the initial light pattern generated by a hyperbolic lens is shown in Figure 2A, a high-quality light-sheet pattern predicted by MATLAB calculation using Green function without phase change boundary is shown in Figure 2B and the corresponding orientation angle of each unit cell implemented in FDTD simulation is illustrated in Figure 2D, and full-wave FDTD simulation result with a

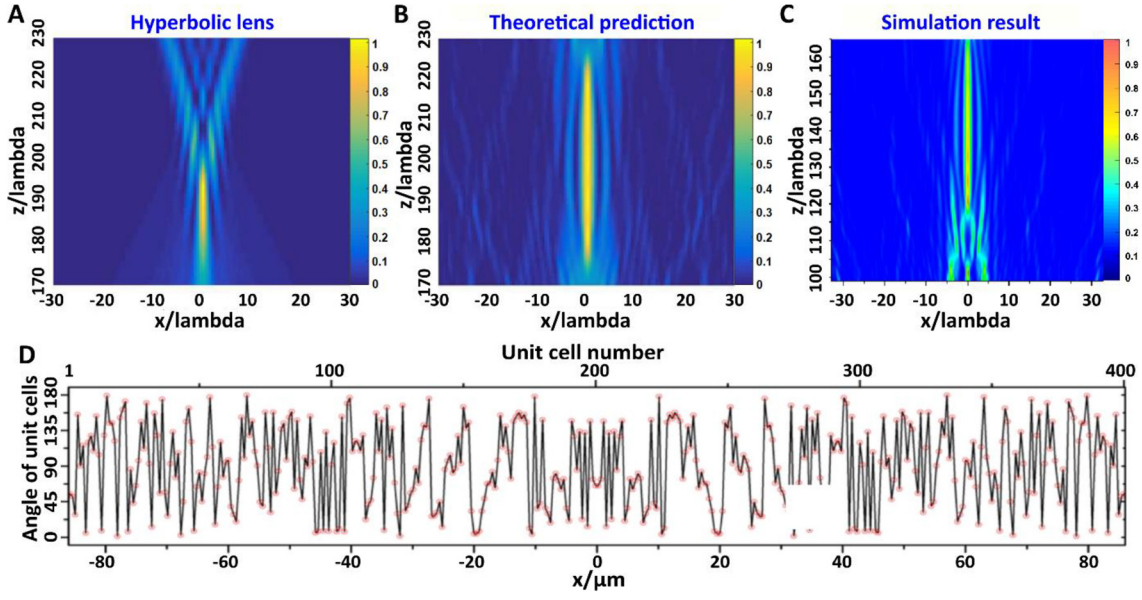

Figure 2: A light pattern generated by using the hyperbolic lens phase profile as initial condition (A); MATLAB-calculated light pat-tern using Green function in a typical case without imposing mutation boundary (B); and orientation angles of 400 unit cells for FDTD simulation (D); Lumerical FDTD simulation result with the phase profile obtained by the phase-change boundary (C).

new phase profile is demonstrated in Figure 2D. Evidently, the optical pattern in Figure 2A grows longer and longer and eventually becomes the pattern shown in Figure 2B after the screened evolution without mutation boundary. As the orientation angle of each PB phase unit cell equals to a half of its additional PB phase, drastic changes in orientation angle in Figure 2D can lead to pronounced phase changes in the PB phase metasurface. Although this phase profile is prohibited for transmission metasurface, the result in Figure 2B exhibits desirable features for a light-sheet pattern that can be reused to produce a new phase profile allowed by transmission metasurface by adding the mutation boundary. The full-wave FDTD simulation result with the new phase profile is shown in Figure 2C, is quite similar to the result predicted by Matlab, insuring the stability and the similar mutation direction under supervision of mutation boundary to the one without mutation boundary. The optical parameters of our design: the refractive index of the ambiance n = 1.33, wavelength λ = 532 nm, number of unit cells 400 for the study of mutation boundary and 3,334 for the later studies, suited for further experimental implementation [4, 6, 8, 9, 39, 63].

We demonstrate the effect of different combinations of (a_1–a_6) with a brief study of different desired effects of light patterns: long length of light sheet as the first case, and significant suppression of side lobes with an excellent resolution (smaller FWHM) as the second case. An example of light sheet with excellent non-diffraction range (about 1.5 mm) is shown in Figure 3A and its corresponding FWHM (8 μm) shown in Figure 3C with coefficient combination: (0.1, 900, 1200, 120,000, 400, and 300); a light sheet with better side lobe suppression and a better resolution but a short non-diffraction range (about 0.5 mm) is shown in Figure 3B and its corresponding FWHM (6 μm) shown in Figure 3D as a comparison, with coefficient combination: (0.1, 900, 30,000, 12,000, 400, and 2,000). Obviously, compared with the first example, a smaller a_4 will result in shorter and thinner main lobe, and bigger a_6 will surely suppress the intensity of side lobe. While the subtle coefficient a_3 has a complicated impact on the pattern shaping of the main lobe. Above all, a bigger a_3 will surely confirm a thinner main lobe, but the effect on the length of the main lobe is difficult to say, as a very long and a much shorter pattern of main lobe may have the same standard variation, once the two patterns follow the Babinet's principle. Consequently, an elaborately selected a_3 can be exploited to give rise to a very long light sheet with a reasonably high resolution of main lobe.

A single light-sheet pattern and two light-sheet pattern extending to a long range 4 mm with reasonable resolution and weak side lobes created by GA machine learning are demonstrated in Figure 4, with Figure 4A the single light sheet pattern with 4 mm long (10,000 λ) non diffracting zone, Figure 4B the corresponding phase profile of the metasurface generated by GA process, Figure 4C the intensity profile in the middle plane of Figure 4A, and Figure 4D the two-light-sheet pattern exhibiting the same non diffracting range as Figure 4A. Obviously, the profile in Figure 4B can hardly be explained by conventional metasurface design principles, though it is slightly similar to the phase profile of an axicon, the noticeable vibrations in the phase of some unit cells should be responsible for the suppression of side modes and the reasonable resolution of the main lobe. Figure 4D shows that the intensities of the

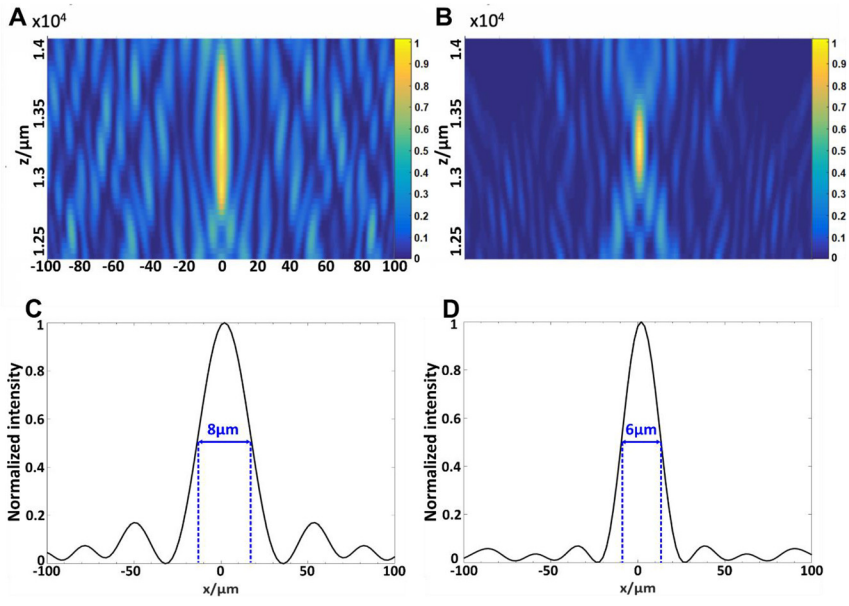

Figure 3: Comparison of different coefficient combinations on the generated light patterns: a combination of coefficient (a_1–a_6) emphasizing the length of the light sheet (A) and the corresponding FWHM shown in (C); and another combination of coefficient (a_1–a_6) emphasizing the side-lobe intensity suppression with reduced FWHM (B) and the corresponding FWHM shown in (D).

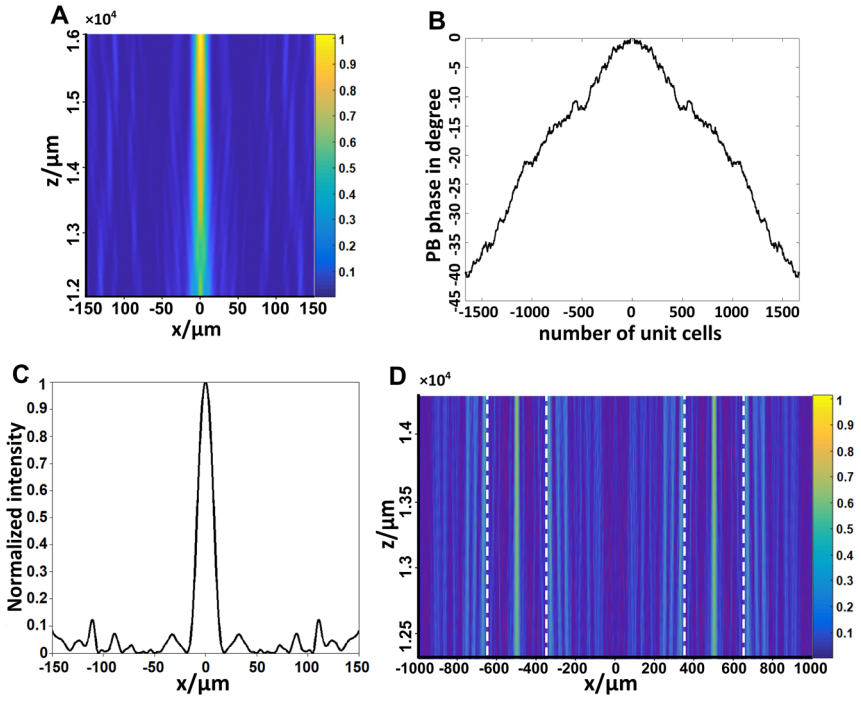

Figure 4: The GA-assisted design of a light-sheet pattern (A) with its corresponding phase profile for each unit cell (B) and the intensity distribution at $z = 14$ mm (C), and a double-light-sheet pattern (D) created by applying the optimized phase profile shown in (B).

side lobes are significantly suppressed to less than <7% of the main peak intensity within the range of ±100 μm, which differs from the intensity profile of Bessel beam and is similar to the result shown in Figure 3D. The phase profile of PB phase metasurface in Figure 4B can be furtherly extended to form the multiplane light sheet with long non-diffracting region and suppressed intensity of the side lobes. An example is shown in Figure 4D where two light sheet beams are created by illuminating the metasurface with the same phase profile in Figure 4B by circularly polarized plane waves. Though some noise residual still exists in Figure 4D, the two light sheets propagating along z direction centered at ±500 μm in x-axis without significant side lobes (rectangular area emphasized by dashed white lines) can unambiguously double the imaging speed of light sheet microscopy by taking image reflected by the two light sheet beams with attenuated side effects of the fluorescence caused by the adjacent tissues illuminated by side lobes of Bessel beam. This two-light-sheet generator designed by GA process can of course be furtherly transformed to create three, even multiplane light sheet pattern with a single metasurface, and will provide a high-speed imaging acquisition several times the conventional light sheet microscopy [57–59] and is free of dithering in the propagation direction than the multiplane light sheet proposed in Reference [64]. Thus, our method demonstrates itself as a promising candidate which can largely accelerate the imaging speed of single illumination light sheet microscopy and greatly simplify the mechanical setup of multiplane light sheet microscopy, and thus, makes a further step towards the practical applications of the multiplane fluorescence light sheet microscopy in the biomedical area.

We further studied the possibility of this method to solve the 3D optical field generated by a 2D PB phase metasurface. In order to fully exploit the capacity of Matlab, another server equipped with AMD Ryzen Threadripper 3990X @ 2.90 GHz (64 cores, 128 threads) and 256 GB memory was used to complete this task. Here, 1000 × 1000 unit cells was chosen to make a trade-off between the metasurface's aperture and the computing capacity of the server: the unit cells number and the monitors number were respectively 300 times and 9 times more than the 2D design due to the dimension increase, while the numerical aperture of the metasurface was kept almost the same. The preliminary result is shown in Figure 5, where the intensity profile in xz (Figure 5A) and yz (Figure 5B) planes exhibit a cylindrical non-diffracting mode within [3.4, 4.6 mm]. The reduction of non-diffraction range to 1.2 mm is attributed to the decrease of the aperture in $x(y)$ direction with the same numerical aperture. Accordingly, the intensity profiles along x and y directions are respectively shown in Figure 5C and Figure 5D, demonstrating a side-mode suppressed pattern quite distinct from 3D Bessel beam, and proving the validity and robustness of our method when extended to 2D metasurface design. Nevertheless, it is worth mentioning that 63 cores and 234 GB memory were occupied by Matlab during the calculation. Thus, if the

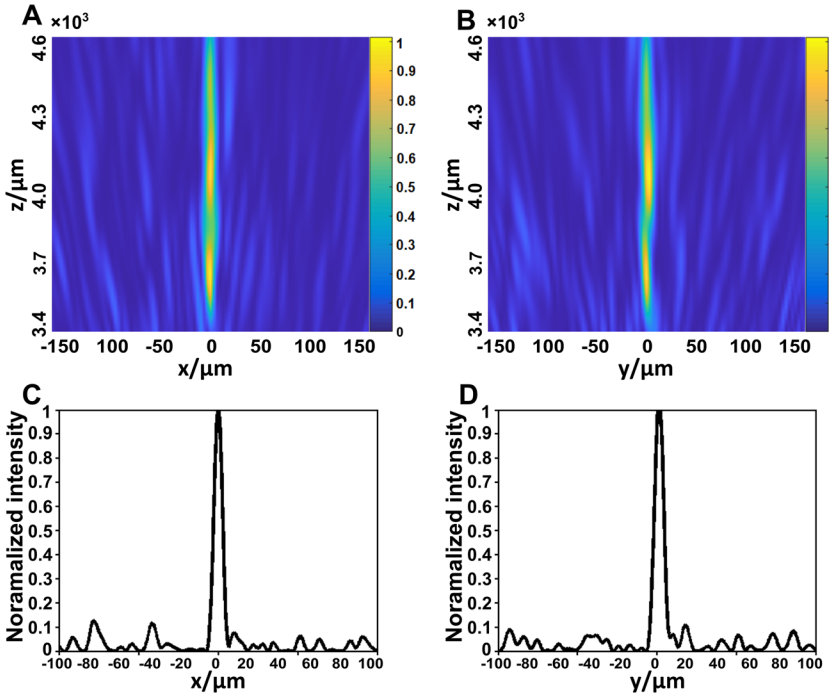

Figure 5: An optimized cylindrical mode generated by a 2D metasurface with (A) intensity profile of the mode in *xz* plane; (B) intensity profile of mode in *yz* plane; (C) intensity distribution along the *x* axis at $z = 4$ mm; and (D) intensity distribution along the *y* axis at $z = 4$ mm.

expected light pattern is, for example, rotational symmetric, an alternative but more viable procedure to design 2D metasurface by using of our GA method with lower computing resource consumption is to first, reduce the dimension of 2D metasurface and seek for the optimal solution of 1D metasurface; then, angularly duplicate the optical 1D metasurface to obtain a rotationally symmetrical 2D metasurface. In such a way, the high-quality optimal 1D metasurface can also be used as building blocks to form the 2D metasurface.

4 Conclusions

In conclusion, we have proposed an optimized GA paradigm for phase-controlled optical metasurface design. This design method has been demonstrated to be capable of solving complex metasurfaces design for generation of customized light sheet patterns. It is based on machine learning without any human intervention, expect for the fitness function providing for the determination of direction of evolution, and shows no relationship with any existing metasurface design and cannot be achieved by conventional analytical solutions or hologram methods. In this study, an elaborately selected fitness function is introduced to evaluate the created light mode with empirical coefficients, a reasonably large mutation rate is chosen to balance the processing efficiency and meanwhile avoid unstable population, and a multi-step hierarchical GA process is created aiming to find the local optima with large mutation extent and subsequently reach the global optimal solution by using a series of small mutation extents. In the meantime, the mutation process is supervised by a mutation boundary function to confirm that the DNA of each child abides the generalized Snell's law.

An optimized single light-sheet pattern and double-light-sheet pattern with 4 mm long non-diffracting zone as proof-of-concept have been presented in this work by tuning the coefficients of fitness function and demonstrate the capability to create multiplane light sheets. A 3D light pattern created by a 2D metasurface is further demonstrated to reveal the potential of our approach for 3D light field manipulation. The obtained results, thus, have proven the validity, robustness and versatility of our GA method. Additionally, another 2D metasurface design method based on 1D metasurface has also been proposed. The GA method studied in this work is quite generic for PB phase metasurface design for optical mode generation and lays a solid foundation for longitudinal light mode formation and paves the way for designing a new family of nano optical devices based on PB phase metasurface design with high transmission efficiency suited for practical biomedical applications in the future.

Acknowledgment: This work was supported by The City University of Hong Kong (Project No. 9360165) and The Hong Kong Polytechnic University (Project Nos. ZVG4 and

1-ZE1B). The authors also acknowledge financial support from Shenzhen Science and Technology Innovation Commission (No. SGDX2019081623281169). The authors are grateful to the Department of Electronic and Information Engineering, The Hong Kong Polytechnic University for their supports as well.

Author contribution: All the authors have accepted responsibility for the entire content of this submitted manuscript and approved submission.

Research funding: This research was funded by The City University of Hong Kong (Project No. 9360165) and The Hong Kong Polytechnic University (Project Nos. ZVG4 and 1-ZE1B). The authors also acknowledge financial support from Shenzhen Science and Technology Innovation Commission (No. SGDX2019081623281169).

Conflict of interest statement: The authors declare no conflicts of interest regarding this article.

Bibliography

[1] N. Yu, and F. Capasso, "Flat optics with designer metasurfaces," *Nat. Mater.*, vol. 13, pp. 139–150, 2014.

[2] W. T. Chen, R. C. Devlin, J. Oh, A. J. Zhu, and F. Capasso, "Metalenses at visible wavelengths diffraction-limited focusing and subwavelength resolution imaging," *Science*, vol. 352, pp. 1190–1194, 2016.

[3] M. Khorasaninejad, A. Y. Zhu, C. Roques-Carmes, et al., "Polarization-insensitive metalenses at visible wavelengths," *Nano Lett.*, vol. 16, pp. 7229–7234, 2016.

[4] H. -H. Hsiao, C. H. Chu, and D. P. Tsai, "Fundamentals and applications of metasurfaces," Small Methods, vol. 1, 2017. Art no. 1600064, https://doi.org/10.1002/smtd.201600064.

[5] Y. Fan, X. Le Roux, A. Korovin, A. Lupu, and A. de Lustrac, "Integrated 2D-graded index plasmonic lens on a silicon waveguide for operation in the near infrared domain," *ACS Nano*, vol. 11, pp. 4599–4605, 2017.

[6] W. T. Chen, A. Y. Zhu, V. Sanjeev, et al., "A broadband achromatic metalens for focusing and imaging in the visible," *Nat. Nanotechnol.*, vol. 13, pp. 220–226, 2018.

[7] S. Wang, P. C. Wu, V. -C. Su, et al., "A broadband achromatic metalens in the visible," *Nat. Nanotechnol.*, vol. 13, pp. 227–232, 2018.

[8] V. C. Su, C. H. Chu, G. Sun, and D.P. Tsai, "Advances in optical metasurfaces: fabrication and applications [Invited]," *Opt. Express*, vol. 26, pp. 13148–13182, 2018.

[9] M. -K. Chen, C. H. Chu, R. J. Lin, et al., "Optical meta-devices: advances and applications," *Jpn. J. Appl. Phys.*, vol. 58, 2019, Art no. SK0801, https://doi.org/10.7567/1347-4065/ab2df0.

[10] A. Arbabi, Y. Horie, M. Bagheri, and A. Faraon, "Dielectric metasurfaces for complete control of phase and polarization with subwavelength spatial resolution and high transmission," *Nat. Nanotechnol.*, vol. 10, pp. 937–943, 2015.

[11] D. Zhang, M. Ren, W. Wu, et al., "Nanoscale beam splitters based on gradient metasurfaces," *Opt. Lett.*, vol. 43, pp. 267–270, 2018.

[12] Y. Fan, X. Le Roux, A. Lupu, and A. de Lustrac, "Ultra-compact on-chip metaline-based 13/16 μm wavelength demultiplexer," *Photonics Res.*, vol. 7, pp. 359–362, 2019.

[13] A. Pors, M. G. Nielsen, and S. I. Bozhevolnyi, "Analog computing using reflective plasmonic metasurfaces," *Nano Lett.*, vol. 15, pp. 791–797, 2015.

[14] H. Babashah, Z. Kavehvash, S. Koohi, and A. Khavasi, "Integration in analog optical computing using metasurfaces revisited: toward ideal optical integration," *J. Opt. Soc. Am. B*, vol. 34, pp. 1270–1279, 2017.

[15] H. Kwon, D. Sounas, A. Cordaro, A. Polman, and A. Alù, "Nonlocal metasurfaces for optical signal processing," *Phys. Rev. Lett.*, vol. 121, 2018, Art no. 173004, https://doi.org/10.1103/PhysRevLett.121.173004.

[16] A. Cordaro, H. Kwon, D. Sounas, A. F. Koenderink, A. Alù, and A. Polman, "High-index dielectric metasurfaces performing mathematical operations," *Nano Lett.*, vol. 19, pp. 8418–8423, 2019.

[17] Y. Zhou, W. Wu, R. Chen, W. Chen, R. Chen, and Y. Ma, "Analog optical spatial differentiators based on dielectric metasurfaces," *Adv. Opt. Mater.*, vol. 8, 2019, Art no. 1901523, https://doi.org/10.1002/adom.201901523.

[18] A. Pors, M. G. Nielsen, and S. I. Bozhevolnyi, "Plasmonic metagratings for simultaneous determination of Stokes parameters," *Optica*, vol. 2, pp. 716–723, 2015.

[19] T. Lepetit, and B. Kanté, "Simultaneous Stokes parameters," *Nat. Photonics*, vol. 9, pp. 709–710, 2015.

[20] A. Basiri, X. Chen, J. Bai, et al., "Nature-inspired chiral metasurfaces for circular polarization detection and full-Stokes polarimetric measurements," *Light Sci. Appl.*, vol. 8, 2019, Art no. 78, https://doi.org/10.1038/s41377-019-0184-4.

[21] L. Huang, X. Chen, H. Mühlenbernd, et al., "Three-dimensional optical holography using a plasmonic metasurface," *Nat. Commun.*, vol. 4, p. 2808, 2013.

[22] D. Wen, F. Yue, G. Li, et al., "Helicity multiplexed broadband metasurface holograms," *Nat. Commun.*, vol. 6, pp. 8241, 2015.

[23] G. Zheng, H. Mühlenbernd, M. Kenney, G. Li, T. Zentgraf, and S. Zhang, "Metasurface holograms reaching 80% efficiency," *Nat. Nanotechnol.*, vol. 10, pp. 308–312, 2015.

[24] L. Wang, S. Kruk, H. Tang, et al., "Grayscale transparent metasurface holograms," *Optica*, vol. 3, pp. 1054–1055, 2016.

[25] J. P. B. Mueller, N. A. Rubin, R. C. Devlin, B. Groever, and F. Capasso, "Metasurface polarization optics: independent phase control of arbitrary orthogonal states of polarization," *Phys. Rev. Lett.*, vol. 118, 2017, Art no. 113901, https://doi.org/10.1103/PhysRevLett.118.113901.

[26] Y. Bao, Y. Yu, H. Xu, et al., "Full-colour nanoprint-hologram synchronous metasurface with arbitrary hue-saturation-brightness control," *Light Sci. Appl.*, vol. 8, p. 95, 2019.

[27] A. C. Overvig, S. Shrestha, S. C. Malek, et al., "Dielectric metasurfaces for complete and independent control of the optical amplitude and phase," *Light Sci. Appl.*, vol. 8, p. 92, 2019.

[28] Y. Hu, X. Luo, Y. Chen, et al., "3D-Integrated metasurfaces for full-colour holography," *Light Sci. Appl.*, vol. 8, p. 86, 2019.

[29] D. Lin, P. Fan, E. Hasman, M. L. Brongersma, "Dielectric gradient metasurface optical elements," *Science*, vol. 345, pp. 298–302, 2014.

[30] E. Karimi, S. A. Schulz, I. De Leon, H. Qassim, J. Upham, and R. W. Boyd, "Generating optical orbital angular momentum at visible wavelengths using a plasmonic metasurface," *Light Sci. Appl.*, vol. 3, 2014, Art no. e167, https://doi.org/10.1038/lsa.2014.48.

[31] M. I. Shalaev, J. Sun, A. Tsukernik, A. Pandey, K. Nikolskiy, and N. M. Litchinitser, "High-efficiency all-dielectric metasurfaces for ultracompact beam manipulation in transmission mode," *Nano Lett.*, vol. 15, pp. 6261–6266, 2015.

[32] F. Aieta, P. Geneve, M. A. Kats, et al., "Aberration-free ultrathin flat lenses and axicons at telecom wavelengths based on plasmonic metasurfaces," *Nano Lett.*, vol. 12, pp. 4932–4936, 2012.

[33] W. T. Chen, M. Khorasaninejad, A. Y. Zhu, et al., "Generation of wavelength- independent subwavelength Bessel beams using metasurfaces," *Light Sci. Appl.*, vol. 6, 2017, Art no. e16259, https://doi.org/10.1038/lsa.2016.259.

[34] Q. Fan, D. Wang, P. Huo, Z. Zhang, Y. Liang, and T. Xu, "Autofocusing Airy beams generated by all-dielectric metasurface for visible light," *Opt. Express*, vol. 25, pp. 9285–9294, 2017.

[35] W. Hao, M. Deng, S. Chen, and L. Chen, "High-efficiency generation of Airy beams with Huygens' metasurface," *Phys Rev. Appl.*, vol. 11, 2019, Art no. 054012, https://doi.org/10.1103/PhysRevApplied.11.054012.

[36] S. Wang, X. Wang, and Y. Zhang, "Simultaneous Airy beam generation for both surface plasmon polaritons and transmitted wave based on metasurface," *Opt. Express*, vol. 25, pp. 23589–23596, 2017.

[37] O. Avayu, O. Eisenbach, R. Ditcovski, and T. Ellenbogen, "Optical metasurfaces for polarization-controlled beam shaping," *Opt. Lett.*, vol. 39, pp. 3892-3895, 2014.

[38] M. Jia, Z. Wang, H. Li, et al., "Efficient manipulations of circularly polarized terahertz waves with transmissive metasurfaces," *Light Sci. Appl.*, vol. 8, p. 16, 2019.

[39] B. H. Chen, P. C. Wu, V. -C. Su, et al., "GaN metalens for pixel-level full-color routing at visible light," *Nano Lett.*, vol. 17, pp. 6345–6352, 2017.

[40] Q. Wu, C. P. Scarborough, D. H. Werner, E. Lier, and X. Wang, "Design synthesis of metasurfaces for broadband hybrid-mode horn antennas with enhanced radiation pattern and polarization characteristics," *IEEE T Antenn. Propag.*, vol. 60, pp. 3594–3604, 2012.

[41] T. J. Cui, M. Q. Qi, X. Wan, J. Zhao, and Q. Cheng, "Coding metamaterials, digital metamaterials and programmable metamaterials," *Light Sci. Appl.*, vol. 3, 2014, Art no. e218. https://doi.org/10.1038/lsa.2014.99.

[42] M. D. Huntington, L. J. Lauhon, and T. W. Odom, "Subwavelength lattice optics by evolutionary design," *Nano Lett.*, vol. 14, pp. 7195–7200, 2014.

[43] L. -H. Gao, Q. Cheng, J. Yang, et al., "Broadband diffusion of terahertz waves by multi-bit coding metasurfaces," *Light Sci. Appl.*, vol. 4, 2015, Art no. e324. https://doi.org/10.1038/lsa.2015.97.

[44] J. Y. Yin, X. Wan, Q. Zhang, and T. J. Cui, "Ultra wideband polarization-selective conversions of electromagnetic waves by metasurface under large-range incident angles," *Sci. Rep.*, vol. 5, 2015, Art no. 12476. https://doi.org/10.1038/srep12476.

[45] S. J. Li, X. Y. Cao, L. M. Xu, et al., "Ultra-broadband reflective metamaterial with RCS reduction based on polarization convertor, information entropy theory and genetic optimization algorithm," *Sci. Rep.*, vol. 5, 2016, Art no. 37409. https://doi.org/10.1038/srep37409.

[46] H. Yang, X. Cao, F. Yang, et al., "A programmable metasurface with dynamic polarization, scattering and focusing control," *Sci. Rep.*, vol. 6, 2016, Art no. 35692, https://doi.org/10.1038/srep35692.

[47] S. Sui, H. Ma, Y. Lv, et al., "Fast optimization method of designing a wideband metasurface using the Pancharatnam-Berry phase," *Opt. Express*, vol. 26, pp. 1443–1451, 2018.

[48] S. Jafar-Zanjani, S. Inampudi, H. Mosallaei, "Adaptive genetic algorithm for optical metasurfaces design," *Sci. Rep.*, vol. 8, 2018, Art no. 11040. https://doi.org/10.1038/s41598-018-29275-z.

[49] Z. Jin, S. Mei, S. Chen, et al., "Complex inverse design of meta-optics by segmented hierarchical evolutionary algorithm," *ACS Nano*, vol. 13, pp. 821–829, 2019.

[50] W. Ma, F. Cheng, and Y. Liu, "Deep-learning-enabled on-demand design of chiral metamaterials," *ACS Nano*, vol. 12, pp. 6326–6334, 2018.

[51] Q. Zhang, C. Liu, X. Wan, et al., "Machine-learning designs of anisotropic digital coding metasurfaces," *Adv. Theory Simul.*, vol. 2, 2018, Art no. 1800132. https://doi.org/10.1002/adts.201800132.

[52] Z. Liu, D. Zhu, K. -T. Lee, A. S. Kim, L. Raju, and W. Cai, "Compounding meta-atoms into metamolecules with hybrid artificial intelligence techniques," *Adv. Mater.*, vol. 32, 2020, Art no. 1904790, https://doi.org/10.1002/adma.201904790.

[53] T. Qiu, X. Shi, J. Wang, et al., "Deep learning: a rapid and efficient route to automatic metasurface design," *Adv. Sci.*, vol. 6, 2019, Art no. 1900128, https://doi.org/10.1002/advs.201900128.

[54] L. Li, H. Ruan, C. Liu, et al., "Machine-learning reprogrammable metasurface imager," *Nat. Commun.*, vol. 10, p. 1082, 2019.

[55] Y. Li, Y. Xu, M. Jiang, et al., "Self-learning perfect optical chirality via a deep neural network," *Phys. Rev. Lett.*, vol. 123, 2019, Art no. 213902, https://doi.org/10.1103/PhysRevLett.123.213902.

[56] L. Li, S. Ya, Q. Ma, et al., "Intelligent metasurface imager and recognizer," *Light Sci. Appl.*, vol. 8, pp. 97, 2019.

[57] J. Huisken, J. Swoger, F. Del Bene, J. Wittbrodt, and E. H. K. Stelzer, "Optical sectioning deep inside live embryos by selective plane illumination microscopy," *Science*, vol. 305, pp. 1007–1009, 2004.

[58] J. Huisken, and D. Y. R. Stainier, "Selective plane illumination microscopy techniques in developmental biology," *Development*, vol. 136, pp. 1963–1975, 2009.

[59] R. M. Power, and J. Huisken, "A guide to light-sheet fluorescence microscopy for multiscale imaging," *Nat. Method*, vol. 14, pp. 306–373, 2017.

[60] M. Born, and E. Wolf, *Principles of Optics: Electromagnetic Theory of Propagation, Interference and Diffraction of Light*, Cambridge University Press, Cambridge, 1999.

[61] T. Roy, S. Zhang, W. Jung, M. Troccoli, F. Capasso, and D. Lopez, "Dynamic metasurface lens based on MEMS technology," *APL Photonics*, vol. 3, 2018, Art no. 021302, https://doi.org/10.1063/1.5018865.

[62] K. Zhang, Y. Yuan, D. Zhang, et al., "Phase-engineered metalenses to generate converging and non-diffractive vortex beam carrying orbital angular momentum in microwave region," *Opt. Express*, vol. 26, pp. 1351–1360, 2018.

[63] S. Wang, P. C. Wu, V. -C. Su, et al., "Broadband achromatic optical metasurface devices," *Nat. Commun.*, vol. 8, p. 187, 2017.

[64] F. Shi, M. Qiu, L. Zhang, E. Y. Lam, and D. Y. Lei, "Multiplane illumination enabled by fourier-transform metasurfaces for high-speed light-sheet microscopy," *ACS Photonics*, vol. 5, pp. 166–1684, 2018.